Hyperspectral coherent anti-Stokes Raman scattering microscopy imaging through turbid medium

Rajan Arora, Georgi I. Petrov, and Vladislav V. Yakovlev
University of Wisconsin – Milwaukee, Department of Physics, 1900 East Kenwood Boulevard, Milwaukee, Wisconsin 53211

Abstract. Coherent Raman microspectroscopy imaging is an emerging technique for noninvasive, chemically specific optical imaging, which can be potentially used to analyze the chemical composition and its distribution in biological tissues. In this report, a hierarchical cluster analysis was applied to hyperspectral coherent anti-Stokes Raman imaging of different chemical species through a turbid medium. It was demonstrated that by using readily available commercial software (Cytospec, Inc.) and cluster analysis, distinct chemical species can be imaged and identified through a rather thick layer of scattering medium. Once the clusters of different chemical composition were distinguished, a phase retrieval algorithm was used to convert coherent anti-Stokes Raman spectra to Raman spectra, which were used for chemical identification of hidden microscopic objects. In particular, applications to remote optical sensing of potential biological threats and to imaging through a layer of skin tissue were successfully demonstrated. © *2011 Society of Photo-Optical Instrumentation Engineers (SPIE)*. [DOI: 10.1117/1.3541796]

Keywords: Raman; coherent anti-Stokes Raman scattering; microscopy; spectroscopy; hyperspectral imaging; scattering.

Paper 10389SSR received Jul. 9, 2010; revised manuscript received Nov. 25, 2010; accepted for publication Dec. 16, 2010; published online Feb. 10, 2011.

1 Introduction

Nonlinear Raman spectroscopy based on coherent anti-Stokes Raman scattering (CARS) spectroscopy is experiencing a renaissance these days sparking new applications and system developments.[1–7] Under proper excitation conditions, CARS microscopy and microspectroscopy is capable of providing a much stronger signal and has the potential for real-time chemical analysis of cells and tissues.[1,6,7] To make a quantitative chemical analysis possible, it is often necessary to collect the extended vibrational spectrum from a selected cell or tissue volume and use sophisticated mathematical algorithms to extract the required information.[8,9] While most of the research efforts are focused on optimizing experimental conditions for excitation and signal collection, we point that most of those efforts were concentrated on identifying objects either in thin samples, or in optically transparent media, thus limiting the area of applications of CARS microspectroscopy. It would be of great advantage to be able to identify chemical composition and molecular structures through a layer of scattering tissue without destroying its structural integrity.[10] This would open a wide window of opportunities to use CARS microspectroscopy for detecting potential biological threats in the mail[11] and deep tissue imaging, which goes beyond the first 100-micron layer of tissue.[12]

One of the least explored advantages of CARS microspectroscopy is its ability to utilize long wavelength excitation, which allows deep tissue imaging. If one looks at absorption and scattering properties of any typical tissue,[13,14] the most significant feature of the scattering coefficient dependence upon the excitation wavelength is in its almost monotonic decay with the increase of the incident wavelength. This is a well-recognized feature in tissue optics, which is widely used in optical diffusion tomography and optical coherence tomography to minimize the effect of light scattering.[15,16] By using a longer wavelength of the incident radiation, light can penetrate deeper into a tissue without experiencing a significant scattering, which affects the signal strength and the resolution of the reconstructed image. The same idea has been recently applied to two-photon fluorescence microscopy, where several groups have attained much deeper imaging capabilities when longer excitation wavelength was employed.[17–19] For example, by utilizing the fundamental wavelength of a Cr:forsterite laser (around 1250 nm), a substantial improvement has been achieved in terms of the imaging depth for the two-photon excitation.

We note that CARS microspectroscopy is almost ideally suitable for deep tissue vibrational Raman imaging. Raman microspectroscopy itself does benefit from a longer excitation wavelength as well. For example, the fluorescence background, which significantly affects the signal-to-noise ratio (SNR) and ambiguity of molecular recognition,[20] is dramatically reduced when a longer excitation wavelength is used. The penetration depth also increases, allowing collection of Raman spectra from deeper layers of tissue. However, in Raman spectroscopy, signal is detected at the wavelength longer than the excitation wavelength, and the use of near-IR excitation often requires cooled InGaAs multichannel detectors,[21] which are not yet widely available in a large multielement format to allow the full Raman spectral acquisition with a good spectral resolution and sensitivity.

At the same time, CARS signal, which is generated at the frequency

$$\omega_{CARS} = \omega_{probe} + (\omega_{pump} - \omega_{Stokes}),$$

Address all correspondence to: Vladislav V. Yakovlev, University of Wisconsin – Milwaukee, Department of Physics, 1900 East Kenwood Boulevard, Milwaukee, WI 53211. Tel: +1-414-229-6163; Fax +1-414-229-3978; E-mail: yakovlev@uwm.edu.

is blue shifted with respect to the frequency of the probe pulse, ω_{probe}, i.e., neither the fluorescence affects the detection, nor the detection sensitivity is an issue for CARS signal detection. Since CARS spectroscopy relies on a nonlinear interaction, its efficiency greatly benefits from the use of high intense laser pulses, which can be potentially harmful to living cells and tissues. However, extensive research indicates that longer excitation wavelength provides a more gentle interaction with tissues, when ultrashort high intensity laser pulses are used.[22–24]

In this report we focus on distinguishing different chemical species using CARS microspectroscopy, when signal is affected by scattering. The problem comes not only in the reduced signal level, but also from the fact that signal generated from different spots might experience substantial variations due to wavelength-dependent scattering both for the incident and generated beams. We propose a solution based on hyperspectral image analysis, which is commonly used in Raman and infrared imaging,[25,26] but, to our best knowledge, has not been employed for CARS microspectroscopy analysis. The key idea of hierarchical cluster analysis is to utilize the similarities of spectral data to separate them into distinct groups. Thus, rather than relying on the absolute intensity of the measured signal at a particular Raman line, algorithm looks for a number of spectral features specific to a particular chemical structure. Using a commercially available software package (Cytospec, Inc., see Ref. 27), we found that it is possible to perform a hierarchical cluster analysis of collected CARS spectra to identify different chemical structures. After identifying different clusters, we employed a Raman retrieval procedure, which has been proven to provide an efficient way of converting information from CARS to Raman spectroscopic data,[7,8] to accurately identify chemical species in each cluster. To illustrate the power of this approach, we first used two relatively simple examples for imaging, in which well-defined objects with strong Raman cross-section were imaged using single vibrational line CARS or Raman imaging and compared with images obtained through the hierarchical cluster analysis of

hyperspectral data. After these validation tests, we utilized the same approach based on hierarchical cluster analysis to identify the presence of dipicolinic acid powder inside a paper envelope, which serves as a powerful example of chemically specific biological threat detection in the mail, since dipicolinic acid is the major compound of bacterial endospores accounting for up to 20% of their weight[7]), and to identify the presence of microcalcifications by imaging and correctly identifying their chemical composition through a millimeter-thick skin layer. Microcalcification has been recognized as one of the potential markers for breast cancer, whose chemical composition has been linked to the grade of the pathological breast disease.[28]

2 Experimental Set-up

We used the optical system shown in Fig. 1, which allowed us to perform broadband (300–3500 cm^{-1}) CARS spectral imaging in a transmission mode. We note that the backscattering, or epi-detection, geometry is more beneficial for *in vivo* tissue imaging; however, in this report we focus primarily on a general understanding of how the wealth of information available through the hypespectral CARS imaging can be treated and used for identification of specific chemical compounds in the presence of light scattering.

For all the spontaneous Raman experiments, we used a home-built Raman microscope, which utilizes the second harmonic of Nd:YVO$_4$ laser (532 nm) for the Raman excitation. We used a liquid-nitrogen-cooled CCD detector (Horiba, Inc.) coupled to a 1/3-meter spectrometer (Horiba, Inc.). An additional holographic Raman notch filter (Kaiser Optical, Inc.) was used to reject the main portion of the residual incident radiation.

For CARS experiments, we used a home-built Nd:YVO$_4$ laser,[29] which with an additional diode-pumped Nd:YVO$_4$ power amplifier was capable of providing as much as 10 μJ per pulse at the repetition rate of about 1 MHz and pulse duration $4-6$ ps. About 20% of the output energy was directed
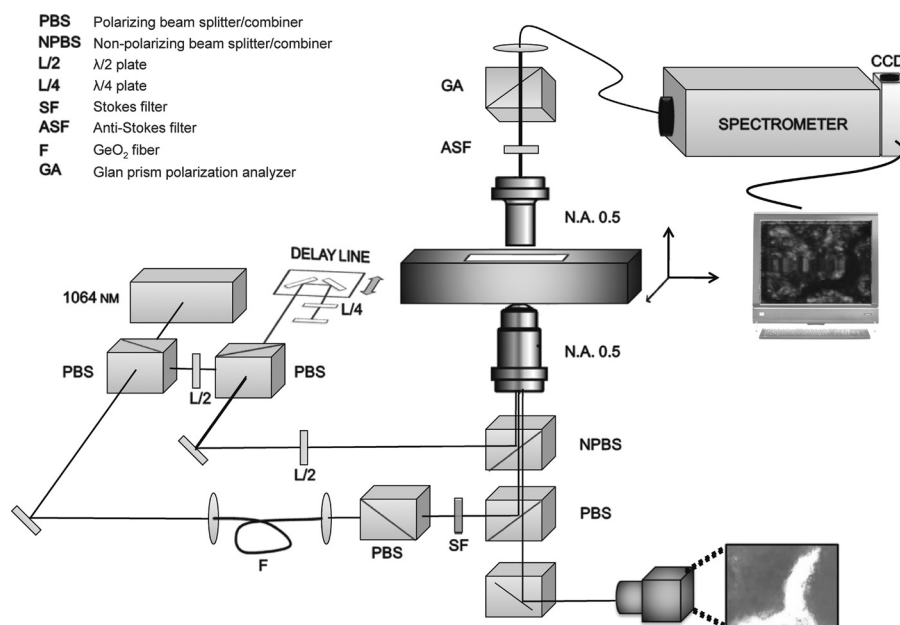

Fig. 1 Schematic diagram of the experimental set-up for CARS microspectroscopy imaging.

into a special Ge-doped fiber to generate a broad, powerful, red-shifted continuum, which was then combined with the rest of the fundamental radiation at 1064 nm to provide a broadband coherent excitation of all vibrational levels, as it was originally proposed and demonstrated in Refs. 23 and 30–31. For all the described experiments, a weak focusing achromatic (in the near-IR part of the spectrum) microscope objective (N.A. = 0.55, Mitutoyo, Inc.) or an aspheric lens (N.A. = 0.3–0.5, Thor Labs, Inc.) was used to focus both incident beams in a geometry close to a collinear. However, such an arrangement limited the bandwidth of CARS spectra to about 1000 cm^{-1}. The signal was collected with an aspheric lens (ThorLabs, Inc.) and directed through a short-pass filter (Omega Optical, Inc.) to a 0.5-meter spectrometer (Horiba, Inc.) with the attached TE-cooled CCD detector (Andor Technology, Inc.). With the full power of the incident beams on a sample (0.1 J/cm^2, which is considered to be safe for this pulse duration and wavelength range[32]), we typically achieved a full saturation of the CCD within an acquisition time as short as 10 ms. All the collected CARS spectra were normalized to the reference CARS spectrum collected from a nonresonant medium (either fused silica window or double distilled water solution), and Raman spectra were retrieved using an algorithm, which is described elsewhere.[7,8,33] In brief, we assumed that the nonresonant tensor component, $\chi_{NR}^{(3)}$, is real and frequency independent and used a maximum entropy method[33] to extract the imaginary part of the resonant tensor component, $\chi_{R}^{(3)}$, which is directly proportional to the Raman signal. The resultant Raman spectrum does not rely on any other assumptions and can be successfully used in both transparent and a highly scattering media;[8] we call such Raman spectrum the "retrieved" Raman spectrum. Those retrieved Raman spectra, unless otherwise is specified, taken at a certain peak value, were used to display the chemically-specific CARS images.

3 Experimental Results

In the first set of experiments, we placed a known, homogeneous microscopic particle on top of a flowing cell (we used a rectangular shaped capillary tube of 2 mm×2 mm cross-section made out of fused silica for this purpose). This way, by flowing a clear solution, like double distilled water, through the cell, we were able to optically image the object to identify its precise location. Then, by flowing a turbid liquid through the cell, the effect of scattering on optical, Raman, and CARS imaging could be evaluated. We used a solution of titania nanoparticles in an alcohol-based solvent, as a scattering medium, whose scattering properties can be controlled by varying the concentration of nanoparticles in solution.[34]

As an object to image, we used a diamond microparticle, which has a very strong Raman scattering cross-section and an isolated vibrational line, which can be utilized for chemical identification (see Fig. 2). We first attempted to use Raman spectroscopy with a 532-nm excitation laser wavelength, but quickly realized that no image contrast [the SNR<1was recorded for any reasonable acquisition time (i.e., than 10 s per data point)] was available for the highest concentrated solution, for which we measured the scattering coefficient of solution to be 20 ± 5 cm^{-1} at 532 nm. Thus, we diluted solution to about 25% of the highest available concentration to achieve a reasonable SNR [about 4,
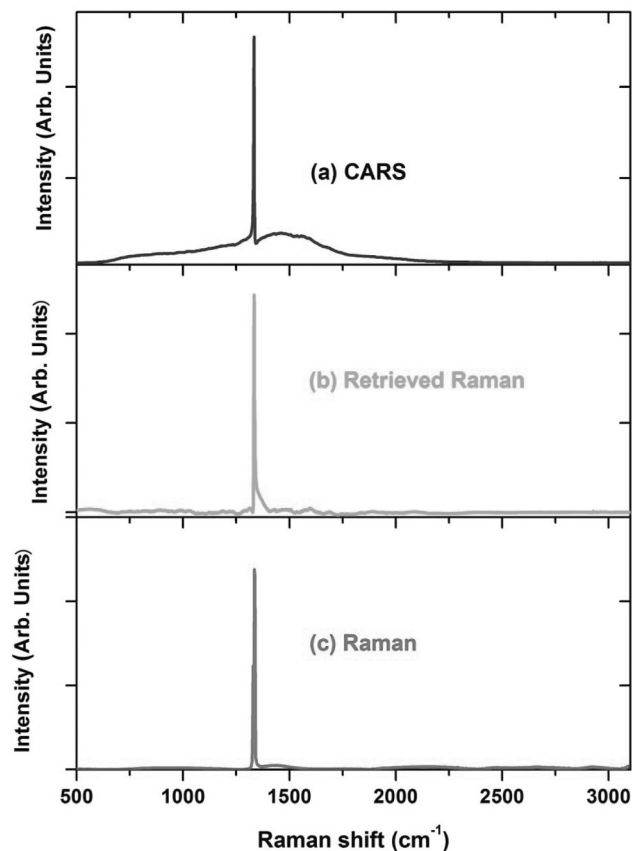

Fig. 2 (a) CARS spectrum, (b) retrieved Raman spectrum, and (c) experimentally measured Raman spectrum of a diamond microparticle.

for the image shown in Fig. 3(c), where each point was taken with a 10-s exposure time) of the Raman image collected at the peak of the diamond strongest Raman line. Optical images [Figs. 3(a) and 3(b)], which were simultaneously recorded using an additional CCD camera, whose spectral detection region was centered at around 800 nm, display a substantially reduced contrast [we estimate the contrast to be over 100 in Fig. 3(a) and about three in Fig. 3(b)] for the case of the turbid media.

On the contrary, even for the highest concentration of scatterers in solution, CARS imaging produced very high contrast imaging (SNR>20, limited primarily by the read-out noise of the camera set-up for high data transfer rate), while optical image contrast was hardly noticeable (see Fig. 4, where the image contrast ratio is less than 1.3). Clearly, both CARS images (for clear and turbid media) are almost indistinguishable even though the amplitude of the CARS signal was reduced by a factor of four due to the reduced intensity of the incident beams on the sample as a result of propagation in a scattering medium (we measured the scattering coefficient of solution at 1064 nm to be 5 ± 2 cm^{-1}). We noted that CARS signal is highly modulated throughout the image, while the diamond microparticle was homogeneous single crystal structure. Clearly, this intensity modulation cannot be attributed to the difference in chemical composition and, most likely, was due to the light scattering inside the particle itself. To deal with this uncertainty of data interpretation, we introduced a hierarchical cluster analysis of the hyperspectral data, which yielded images displayed in Fig. 5, for
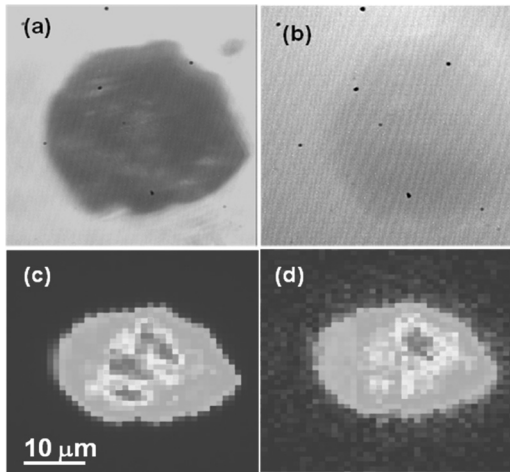
Fig. 3 (a) Microscopic optical image of a diamond microparticle through a distilled water solution, (b) microscopic optical image of a diamond microparticle through a solution of titania nanoparticles (25% of the maximum concentration), (c) chemically-specific microscopic Raman image of a diamond microparticle through a distilled water solution, (d) chemically-specific microscopic Raman image of a diamond microparticle through a solution of titania nanoparticles (25% of the maximum concentration). Images (a) and (b) are shown at approximately the same scale as (c) and (d).

which we assumed two different chemicals/clusters ("diamond" and "no diamond"). If the third cluster is artificially added into consideration, it results in a thin border line, where Raman signal from the diamond particle is substantially reduced. CARS and retrieved Raman spectra from the "diamond" cluster were indistinguishable from the ones shown in Fig. 2.

We realized the oversimplification of our experimental arrangement by noting that fused silica cell provided a substantial spatial displacement of the imaged object and the scattering medium, which produces a substantial background for Raman
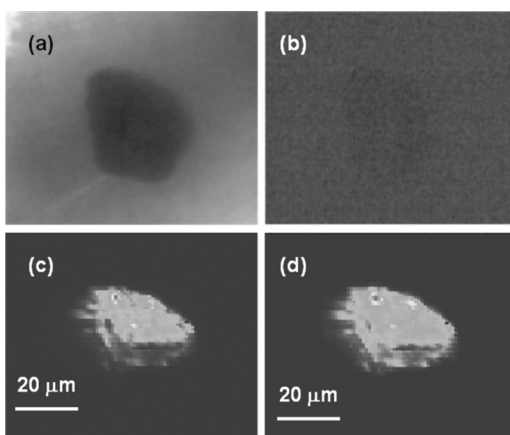

Fig. 4 (a) Microscopic optical image of a diamond microparticle through a distilled water solution, (b) microscopic optical image of a diamond microparticle through a solution of titania nanoparticles (maximum concentration), (c) chemically-specific microscopic CARS image of a diamond microparticle through a distilled water solution, (d) chemically-specific microscopic CARS image of a diamond microparticle through a solution of titania nanoparticles (maximum concentration). Images (a) and (b) are shown at approximately the same scale as (c) and (d).
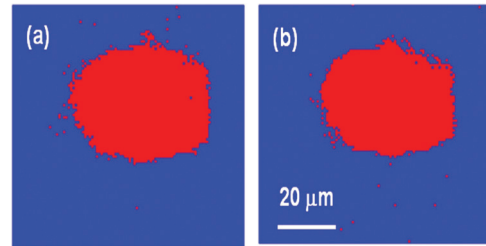
Fig. 5 Cluster images of diamond through (a) a distilled water solution and (b) a scattering solution: red – "diamond," blue – "no diamond." (Color online only.)

imaging. Fused silica does not have any significant Raman scattering in the spectral range of interest and does not introduce any background in the CARS microspectroscopy imaging. Such a situation rarely occurs in practice; however, our initial results confirm our original hypothesis that CARS imaging performed with long-wavelength excitation provides a means of generating sufficiently strong CARS signals through a scattering medium.

As a second example, we considered imaging an object through an ordinary paper tissue (approximately, $100 - \mu m$ thick). This is a typical situation in remote biosensing, when a biologically hazardous object is hidden in a paper envelope and delivered through regular mail. We used a trans-stilbene powder as a target molecular specimen. Stilbenes and its derivatives
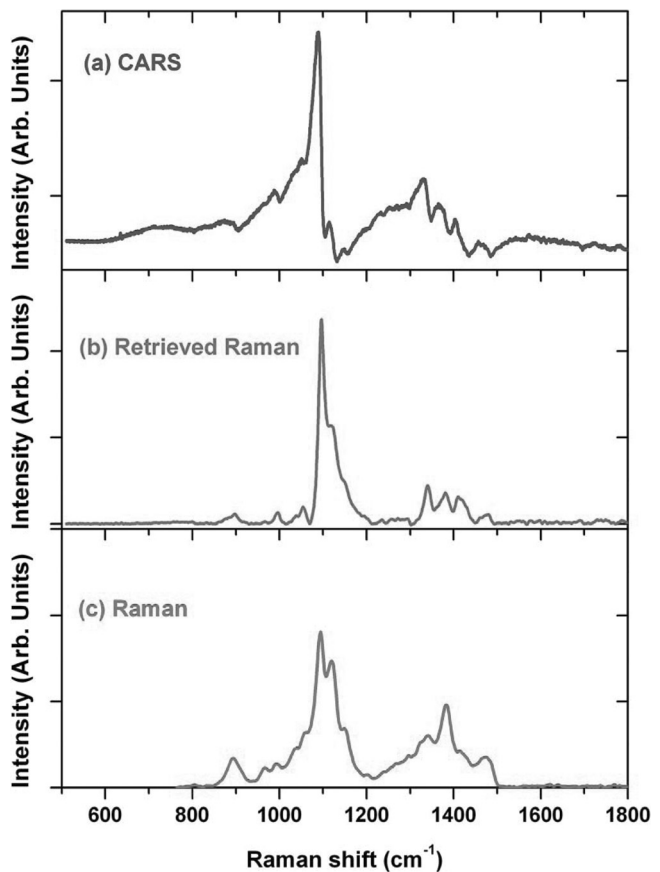
Fig. 6 (a) CARS spectrum, (b) retrieved Raman spectrum, and (c) experimentally measured Raman spectrum of a tissue paper used in experiments.
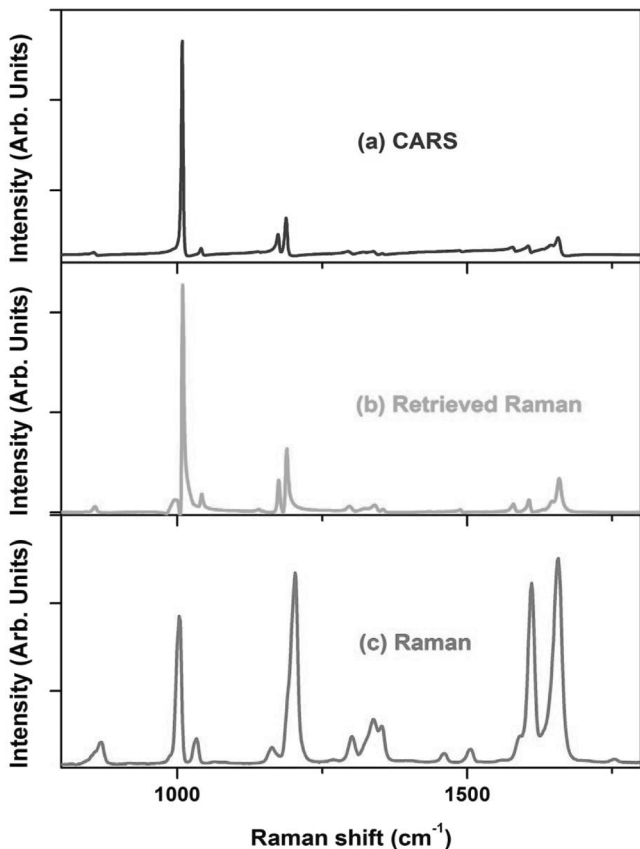
Fig. 7 (a) CARS spectrum, (b) retrieved Raman spectrum, and (c) experimentally measured Raman spectrum of a trans-stilbene powder used in experiments.

are used to produce some nonsteroidal synthetic estrogens and are often used as a part of dietary supplements.[35] Trans-stilbene powder was purchased from Aldrich-Sigma, Inc. (Milwaukee, WI, USA) and was further powderized to make particles less than 5 micron in diameter. Those particles were selected by passing through a 5-μm mesh, and their powder was distributed on a paper surface and covered with another sheet of paper before being imaged by our instrument. Both Raman and CARS spectra of trans-stilbene and paper, used in our experiments, are shown in Figs. 6 and 7, respectively. Relatively large Raman cross-section of trans-stilbene and its distinct Raman features allowed chem-
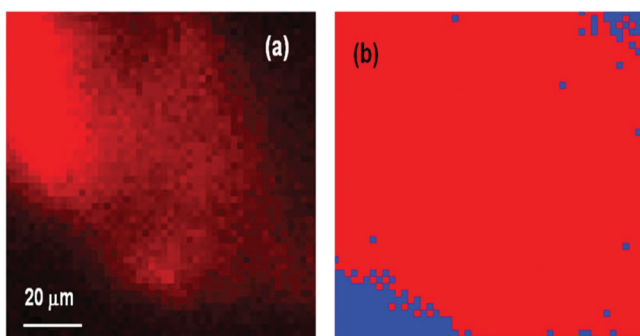

Fig. 8 Chemically-specific (a) and cluster (red – "trans-stilbene," blue – "no trans-stilbene") (b) CARS images of trans-stilbene powder through a paper tissue. (Color online only.)
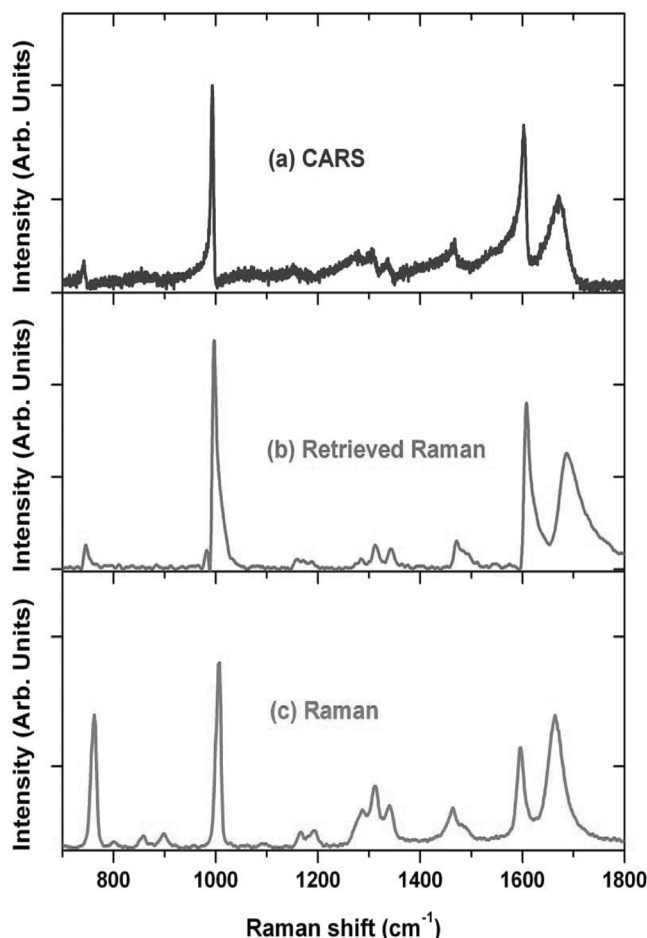

Fig. 9 (a) CARS spectrum, (b) retrieved Raman spectrum, and (c) experimentally measured Raman spectrum of a dipicolinic acid.

ical imaging of this powder through a double layer of paper [see Fig. 8(a); we used Raman line at around 1000 cm^{-1} as a "marker" for stilbene powder presence]. However, the hierarchical cluster analysis of the same hyperspectral data sets exhibited that trans-stilbene was present almost everywhere across the whole field of view [see Fig. 8(b)], which was consistent with the way the sample was prepared. This example exhibits a limitation of single line Raman/CARS imaging, which relies on the intensity alone of a specific line and might underestimate the presence of a certain chemical composition in the inspection volume and/or overestimate the structural inhomogeneities of its distribution.

To illustrate the potential power of imaging biological threats in a unopened envelope, we placed a powder of dipicolinic acid, which is considered to be a native chemical marker for bacterial spores, such as anthrax, in an envelope and attempted to image its distribution. Dipicolinic acid powder was purchased from Sigma-Aldrich, Inc. (Milwaukee, WI, USA). Raman and CARS spectra of dipicolinic acid are shown in Fig. 9. An envelope filled with a powder was placed on a microscopic stage and the focal point of the incident beam was positioned several hundred microns below the front paper surface. CARS spectra were collected at each point in the plane with a 100-ms acquisition time at the incident energy level of 0.1 J/cm^2 to avoid any damage to the paper material. The resulted hierarchical cluster
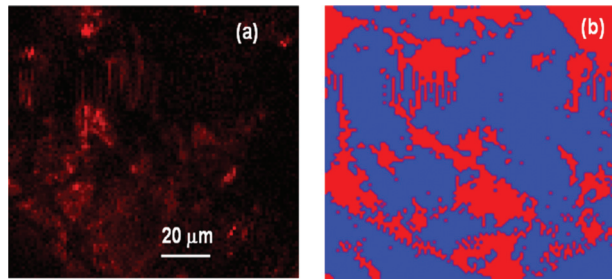
Fig. 10 Chemically-specific (a) and cluster (red – "dipicolinc acid," blue – "no dipicolinc acid") (b) CARS images of dipicolinic acid powder through a paper tissue. (Color online only.)

image, which shows simultaneous imaging of paper material and dipicolinic acid powder, is compared to the chemical image, obtained from the same data set, in Fig. 10. We used a Raman line at around 1600 cm^{-1} as a "chemical marker" for dipicolinic acid powder presence. While both images indicate the presence of dipicolinic acid, in our opinion, the hierarchical cluster analysis is better suited for this purpose, since it allows a clear separation of a foreign substance prior to any knowledge of the nature of this substance, while a chemical image based on a single Raman line tends to underestimate the amount of dipicolinic acid powder present in the envelope.
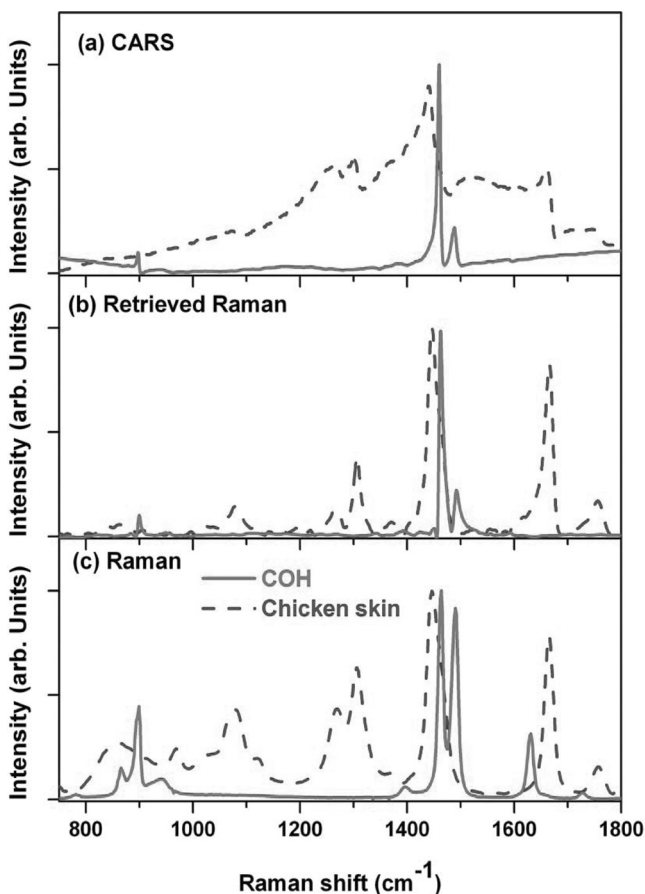

Fig. 11 (a) CARS spectrum, (b) retrieved Raman spectrum, and (c) experimentally measured Raman spectrum of a skin (solid, red line) and microcalcifications (dashed, blue line).

Finally, we investigated the ability of CARS microspectroscopy to chemically image specific chemical structures through a layer of a skin tissue. Xie et al. have demonstrated the ability of CARS microspectroscopy to image lipids *in vivo*;[1] however, most of the chemicals of interest do not have such a strong CARS or Raman signal as lipids do and their spectral features are often overlapping with those of skin, which is mostly composed of fat and collagen. We purchased a chicken skin in a supermarket and used it as a layer of material covering calcium oxalate hydroxide (COH) microcrystals distributed on a glass surface. Calcium oxalate hydroxide solution was purchased from Sigma-Aldrich, Inc. (Milwaukee, WI, USA) and was evaporated prior to use as a solid powder. The skin thickness considerably varied across the area of the sample, but was at least 1-mm-thick in its thinnest region. Imaging and chemical classification of microcalcifications is important for breast cancer diagnostics and identification of the breast tumor margins during breast surgery.[28] Generally, COH microcalcification are considered harmless, but the x ray machines are unable to distinguish those from the other type of microcalcifications, which contain calcium hydroxyapatite. Clearly, there is a great potential for CARS microspectroscopy to provide guidance to medical doctors by identifying the chemical composition of those microcalcifications. The CARS and Raman spectra of those microcalcifications and skin are shown in Fig. 11, and chemical and hierarchical cluster images are shown in Fig. 12. Given the congested spectrum of the skin, we provided to chemically-specific images: the first one [Fig. 12(a)] is based on the intensity of one of the strongest COH Raman lines around 1500 cm^{-1}, the other one [Fig. 12(b)] was taken by subtracting the signal intensity at around 1400 cm^{-1}, where there is no significant COH-specific Raman line present, from the intensity of the COH-specific Raman line. While all those images clearly demonstrate the ability of CARS microspectroscopy to identify the presence of specific chemical structures through a chemically and structurally complex skin layer, hierarchical cluster analysis provides a better judgment, since cluster selection is based on the full vibrational spectrum.

4 Discussion

We present first results on using hierarchical cluster analysis for hyperspectral CARS imaging through turbid media. By imaging microscopic objects hidden below a highly scattering material, we mimicked practical situations of chemically-specific imaging of tissues *in vivo* and detection of biological threats in the mail. The advantage of using hyperspectral analysis is obvious: rather than relying on a single vibrational frequency, a full vibrational spectrum is considered. We anticipate that by considering more complex systems, an increasing number of clusters has to be considered. So far, we have been able to successfully manage up to four different clusters[11] providing a chemical identification for each of them. However, in many practical biomedical implementations, it is important to identify tumor borders and two or three clusters should be considered.

At the same time, we demonstrated the ability of CARS microspectroscopy to image and chemically identify objects below several hundred of microns into turbid medium. This became possible due to the longer excitation wavelength and significantly reduced scattering, as compared to the visible and
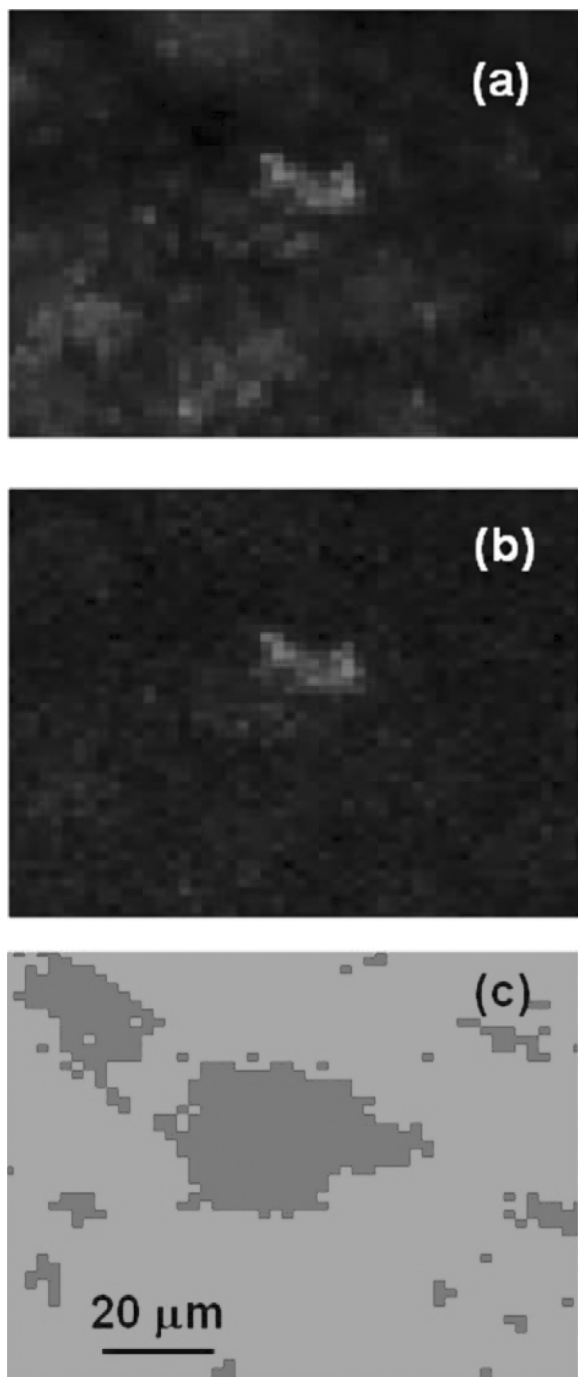
Fig. 12 Chemically-specific single-peak (a), chemically-specific single-peak with a background subtraction (see the text for more details) (b), and cluster (red – "microcalcifications," green – "no microcalcifications") (c) CARS images of microcalcifications through a chicken skin. (Color online only.)

even the near-IR (700–800 nm) excitation. With the newest version of CytoSpec software (see Ref. 27), a real-time analysis of images becomes possible using a moderately powered computer workstation opening a window of opportunities for a practical implementation of chemically specific CARS microspectroscopy imaging into biomedical research and diagnostics.

References

1. C. L. Evans, E. O. Potma, M. Puoris'haag, D. Cote, C. P. Lin, and X. S. Xie, "Chemical imaging of tissue *in vivo* with video-rate coherent anti-Stokes Raman scattering microscopy," *Proc. Natl. Acad. Sci. U.S.A.* **102**, 16807–16812 (2005).
2. M. O. Scully, G. W. Kattawar, R. P. Lucht, T. Opatrny, H. Pilloff, A. Rebane, A. V. Sokolov, and M. S. Zubairy, "FAST CARS: Engineering a laser spectroscopic technique for rapid identification of bacterial spores," *Proc. Natl. Acad. Sci. U.S.A.* **99**, 10994–11001 (2002).
3. C. L. Evans and X. S. Xie, "Coherent Anti-Stokes Raman Scattering Microscopy: Chemical Imaging for Biology and Medicine," *Annu. Rev. Anal. Chem.* **1**, 883–909 (2008).
4. C. Krafft, A. A. Ramoji, C. Bielecki, N. Vogler, T. Meyer, D. Akimov, P. Rosch, M. Schmitt, B. Dietzek, I. Petersen, A. Stallmach, and J. Popp, "A comparative Raman and CARS imaging study of colon tissue," *J. Biophotonics* **2**, 303–312 (2009).
5. G. W. Jones, D. L. Marks, C. Vinegoni, and S. A. Boppart, "High-spectral-resolution coherent anti-Stokes Raman scattering with interferometrically detected broadband chirped pulses," *Opt. Lett.* **31**, 1543–1545 (2006).
6. H. W. Li, D. A. Harris, B. Xu, P. J. Wrzesinski, V. V. Lozovoy, and M. Dantus, "Coherent mode-selective Raman excitation towards standoff detection," *Opt. Express* **16**, 5499–5504 (2008).
7. G. I. Petrov, R. Arora, V. V. Yakovlev, X. Wang, A. V. Sokolov, and M. O. Scully, "Comparison of coherent and spontaneous Raman microspectroscopies for noninvasive detection of single bacterial endospores," *Proc. Natl. Acad. Sci. U.S.A.* **104**, 7776–7779 (2007).
8. R. Arora, G. I. Petrov, and V. V. Yakovlev, "Analytical application of nonlinear Raman microspectroscopy," *J. Mod. Opt.* **55**(19–20), 3237–3254 (2008).
9. P. D. Chowdary, W. A. Benalcazar, Z. Jiang, D. M. Marks, and S. A. Boppart, "High speed nonlinear interferometric vibrational analysis of lipids by spectral decomposition," *Anal. Chem.* **82**, 3812–3818 (2010).
10. H. F. Wang, T. B. Huff, Y. Fu, K. Y. Jia, and J. X. Cheng, "Increasing the imaging depth of coherent anti-Stokes Raman scattering microscopy with a miniature microscope objective," *Opt. Lett.* **32**, 2212–2214 (2007).
11. G. I. Petrov, V. V. Yakovlev, A. V. Sokolov, and M. O. Scully, "Detection of Bacillus subtilis spores in water by means of broadband coherent anti-Stokes Raman spectroscopy," *Opt. Express* **113**, 9537–9542 (2005).
12. F. Helmchen and W. Denk, "Deep tissue two-photon microscopy," *Nat. Methods* **2**, 932–940 (2005).
13. W. F. Cheing, S. A. Prahl, and A. J. Welch, "A review of the optical properties of biological tissues," *IEEE J. Quantum Electron.* **26**, 2166–2185 (1990).
14. T. L. Troy and S. N. Thennadil, "Optical properties of human skin in the near infrared wavelength range of 1000 to 2200 nm," *J. Biomed. Opt.* **6**, 167–176 (2001).
15. U. Sharma, E. W. Chang, and S. H. Yun, "Long-wavelength optical coherence tomography at 1.7-μm for enhanced imaging depth," *Opt. Express* **16**, 19712–19723 (2008).
16. H. Dehghani, B. W. Pogue, S. P. Polack, and K. D. Paulsen, "Multi-wavelength three-dimensional near-infrared tomography of the breast: initial simulation, phantom, and clinical results," *Appl. Opt.* **42**, 135–145 (2003).
17. S. W. Chu, I. H. Chen, T. M. Liu, P. C. Chen, C. K. Sun, and B. L. Lin, "Multimodal nonlinear spectral microscopy based on a femtosecond Cr:forsterite laser," *Opt. Lett.* **26**, 1909–1911 (2001).

18. M. Balu, T. Baldacchini, J. Carter, T. B. Krasieva, R. Zadoyan, and B. J. Tromberg, "Effect of excitation wavelength on penetration depth in nonlinear optical microscopy of turbid media," *J. Biomed. Opt.* **14**, 010508 (2009).
19. D. Kobat, M. E. Durst, N. Nishimura, A. W. Wong, C. B. Schaffer, and C. Xu, "Deep tissue multiphoton microscopy using longer wavelength excitation," *Opt. Express* **17**, 13354–11364 (2009).
20. V. V. Yakovlev, "Time-gated confocal Raman microscopy," *Spectroscopy* **22**, 34–41 (2007).
21. Y. K. Min, T. Yamamoto, E. Kohda, T. Ito, and H. Hamaguchi, "1064 nm near-infrared multichannel Raman spectroscopy of fresh human lung tissues," *J. Raman Spectrosc.* **36**, 73–76 (2005).
22. J. M. Squirrell, D. L. Wokosin, J. G. White, and B. D. Bavister, "Long-term two-photon fluorescence imaging of mammalian embryos without compromising viability," *Nat. Biotechnol.* **17**, 763–766 (1999).
23. V. V. Yakovlev, "Advanced instrumentation for nonlinear Raman microscopy," *J. Raman Spectrosc.* **34**(12), 957–964 (2003).
24. I.-H. Chen, S.-W. Chu, C.-K. Sun, P.-C. Cheng, and B.-L. Lin, "Wavelength dependent damage in biological multi-photon confocal microscopy: A micro-spectroscopic comparison between femtosecond Ti:sapphire and Cr:forsterite laser sources," *Opt. Quantum Electron.* **34**, 1251–1266 (2004).
25. D. C. Fernandez, R. Bhargava, S. M. Hewitt, and I. W. Levin, "Infrared spectroscopic imaging for histopathologic recognition," *Nat. Biotechnol.* **23**, 469–474 (2005).
26. M. Mijkovic, T. Chernenko, M. J. Romeo, B. Bird, C. Matthaus, and M. Diem, "Label-free imaging of human cells: algorithms for image reconstruction of Raman hyperspectral datasets," *Analyst* **135**, 2002–2013 (2010).
27. P. Lasch, W. Haensch, D. Naumann, and M. Diem, "Imaging of colorectal adenocarcinoma using FT-IR microspectroscopy and cluster analysis," *Biochim. Biophys. Acta* **1688**, 176–186 (2004).
28. R. Baker, K. D. Rogers, N. Shepherd, and N. Stone, "New relationships between breast microcalcifications and cancer," *Br. J. Cancer* **103**, 1034–1039 (2010).
29. G. I. Petrov, V. V. Yakovlev, and N. I. Minkovski, "Broadband continuum-generation of the output of high-energy diode-pumped picosecond Nd:YVO$_4$ laser" *Opt. Commun.* **229**, 441–445 (2004).
30. V. Yakovlev, "Advances in real-time nonlinear Raman microscopy," *Proc. SPIE* **4254**, 97–105 (2001).
31. G. I. Petrov and V. V. Yakovlev, "Enhancing red-shifted white-light continuum generation in optical fibers for applications in nonlinear Raman microscopy," *Opt. Express* **13**(4), 1299–1306 (2005).
32. S. S. Kumru, C. P. Cain, G. D. Noojin, M. F. Cooper, M. L. Imholte, D. J. Stolarski, D. D. Cox, C. C. Crane, and B. A. Rockwell, "ED50 study of femtosecond terawatt laser pulses on porcine skin," *Lasers Surg. Med.* **37**, 59–63 (2005).
33. E. M. Variainen, "Phase retrieval approach for coherent anti-Stokes Raman scattering spectrum analysis," *J. Opt. Soc. Am. B* **9**, 1209–1214 (1992).
34. C. Das, A. Trivedi, K. Munaim, and T. Vo-Dinh, "Short pulse laser propagation through tissues for biomedical imaging," *J. Phys. D: Appl. Phys.* **36**, 1–8 (2003).
35. G. Likhtenshtein, *Stilbenes: Applications in Chemistry, Life Sciences and Materials Science*, Wiley-VCH, Weinheim (2010).